ATMOSPHERIC SCIENCE LETTERS
Atmos. Sci. Let. **11**: 7–12 (2010)
Published online 8 January 2010 in Wiley InterScience
(www.interscience.wiley.com) **DOI:** 10.1002/asl.245

RMetS
Royal Meteorological Society

Observed ENSO teleconnections with the South American monsoon system

V. Krishnamurthy[1,2]* and Vasubandhu Misra[3]

[1]*Center for Ocean-Land-Atmosphere Studies, Institute of Global Environment and Society, Calverton, MD, USA*
[2]*Department of Atmospheric, Oceanic and Earth Sciences, George Mason University, Fairfax, VA, USA*
[3]*Department of Meteorology and Center for Ocean-Atmospheric Prediction Studies, Florida State University, Tallahassee, FL, USA*

**Correspondence to:*
V. Krishnamurthy, Center for Ocean-Land-Atmosphere Studies, Institute of Global Environment and Society, 4041 Powder Mill Road, Suite 302, Calverton, MD 20705, USA.
E-mail: krishna@cola.iges.org

Received: 14 July 2009
Revised: 29 September 2009
Accepted: 29 September 2009

Abstract

This study establishes from observations that there exists a spatially coherent and seasonally persistent association of El Niño and Southern Oscillation(ENSO) with the South American monsoon variability over a large region that includes central-east part of South America. This result is confirmed using both remote sensing data of outgoing long-wave radiation and *in situ* rain gauge observations independently. This slowly varying atmospheric pattern has very high daily correlation with the sea surface temperature(SST) over the tropical Pacific and Indian Oceans. The December-to-March seasonal mean of the rainfall is often determined by this ENSO-related pattern. Copyright © 2010 Royal Meteorological Society

Keywords: **ENSO; South America; monsoon variability; sea surface temperature**

1. Introduction

The tropical South American climate has a robust annual cycle of precipitation and is often compared to the monsoon systems around the globe (Zhou and Lau, 1998; Vera *et al*., 2006). However, the prediction of the tropical South American rainfall variability on seasonal to interannual time scales has been rather elusive (Vera *et al*., 2006). This shortcoming has been attributed to the absence of a strong relation between slowly varying tropical sea surface temperature (SST) and the South American summer seasonal rainfall (Liebmann and Marengo, 2001; Liebmann *et al*., 2001; Carvalho *et al*., 2002; Grimm, 2003, 2004). Related observational studies have indicated that the influence of El Niño and Southern Oscillation (ENSO) over central-east South America (CESA) is subseasonal in nature (Grimm, 2003, 2004). This feature was attributed to the competition between remote ENSO forcing and regional processes that cause abrupt change in the rainfall anomalies from one month to the other in the austral summer season. It was concluded that seasonal anomalies (which tend to smooth out these subseasonal anomalies of rainfall) over southeastern Brazil do not show a significant relationship with ENSO.

The present study isolates the interannual variability of precipitation and convection over a large part of South America by applying multichannel singular spectrum analysis (MSSA) on daily values of both remotely sensed outgoing long-wave radiation (OLR) and *in situ* (gridded) rain gauge observations. It will be shown that the leading daily patterns obtained for the two data sets are consistent with each other and exhibit very similar type of ENSO modulation over CESA which covers a large part of Brazil.

2. Data and methodology

The daily mean OLR data on a 2.5° longitude × 2.5° latitude grid were obtained from the National Oceanic and Atmospheric Administration (NOAA) for the period 1979–2007 (Liebmann and Smith, 1996). The rain gauge observations on a 1° longitude × 1° latitude grid for 1979–2005 came from Version SA19 of Liebmann and Allured (2005). This study has also used the newly developed daily Optimally Interpolated SST Version 2 dataset from NOAA (Reynolds *et al*., 2007). The daily values of the SST on 0.25° longitude × 0.25° latitude grid were obtained for the period 1982–2007. The daily climatology, calculated as the mean of the total daily values for each calendar day, was subtracted from the total field to obtain the daily anomalies.

To extract distinct space–time patterns of convection and rainfall over the CESA region, MSSA has been applied to the respective daily data. A review by Ghil *et al*. (2002) describes the mathematical formulation and the technique. The space–time structure of oscillatory modes and persisting modes is obtained in a manner similar to those found in a recent study of the Indian monsoon region (Krishnamurthy and Shukla, 2007). The application of MSSA to data at L grid points specified at N discrete times using lags from 0 to $M-1$ yields LM eigenvalues and LM eigenvectors. The eigenvectors are the space–time empirical orthogonal function (ST-EOF), each consisting of M

sequence of maps. Each corresponding space–time principal component (ST-PC) is of time length $N' = N - M + 1$, and the eigenvalues describe the variance explained. The original time series is expressed as a sum of reconstructed components (RC), each constructed from the lagged maps of the ST-EOF and the ST-PC of the corresponding eigenmode (Ghil *et al*., 2002).

The correlation values presented here have undergone statistical tests at 5% significance level. Since the daily time series has varying persistence, the degrees of freedom are properly estimated by taking into account the e-folding times of their autocorrelation functions.

3. Results

3.1. Correlation of SST with OLR and rainfall anomalies of CESA region

The OLR and precipitation anomalies are area averaged over the CESA region [60 °W–40 °W, 20 °S–5 °S, Figure 1(a)], the same area used by Vera *et al*. (2006) to study their relation with the SST anomalies. This area average will be referred to as the CESA index, hereafter. The point correlation between daily OLR CESA index and contemporaneous daily SST anomalies during December–January–February–March (DJFM) of 1982–2007 is shown in Figure 1(a). The correlations are very weak with statistically significant positive values appearing mainly over the equatorial Pacific Ocean and much of the Atlantic Ocean. However, there is no strong spatial structure that can be related to ENSO. Similar point correlation of CESA precipitation index with SST anomalies shown in Figure 1(b) reveals no discernible relation between CESA region precipitation and Pacific SST.

The correlations between seasonally averaged CESA index and seasonal SST anomalies, however, are found to be stronger because of the absence of subseasonal variations. The point correlations between DJFM seasonal averages of OLR CESA index and SST anomalies show a spatial structure with ENSO signature over the eastern equatorial Pacific (Figure 1(c)). Although the correlation values are higher, the statistically significant correlations appear only in small regions in the Pacific. A large region of the Atlantic Ocean shows significant correlation. Similar point correlations between DJFM seasonal precipitation CESA index and SST anomalies shown in Figure 1(d) resemble the OLR correlations in Figure 1(c) to some extent in the Pacific but with opposite sign. However, the correlation over the North Atlantic Ocean is considerably reduced. An examination of Figure 1, taking into consideration the statistically significant correlations, may lead one to conclude that the tropical Pacific SST is not related to OLR or precipitation in the CESA region except possibly with seasonally averaged OLR, similar to the results of Liebmann *et al*. (2001) and Carvalho *et al*. (2002).

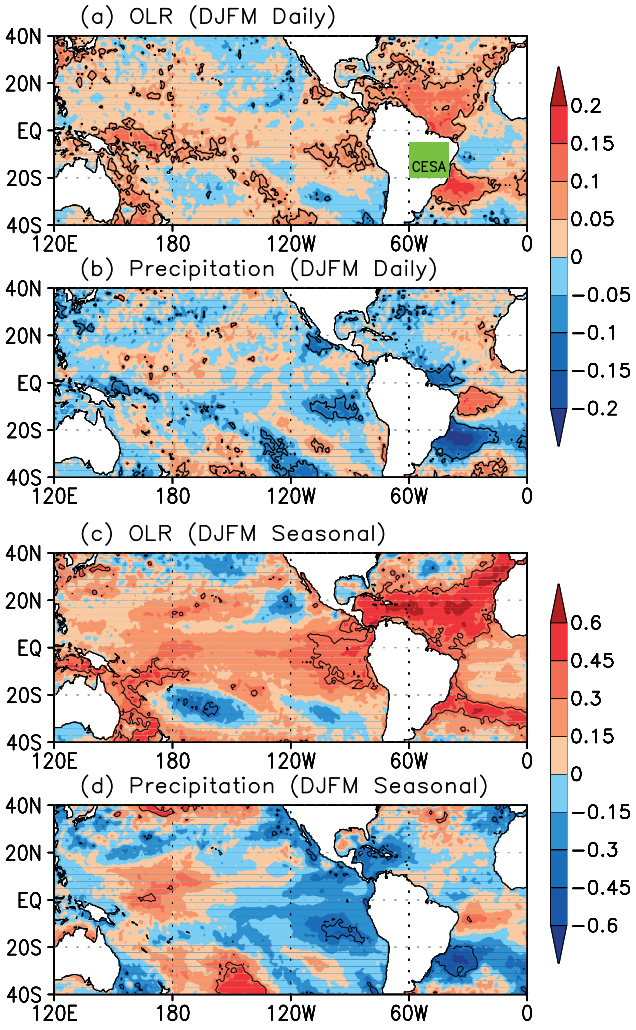

Figure 1. Point correlation of daily (a) OLR anomalies and (b) precipitation anomalies area averaged over the CESA region [60 °W–40 °W, 20 °S–5 °S, shown as green box in (a)] with daily SST anomalies. The periods for OLR and precipitation correlations are DJFM 1982–2007 and DJFM 1982–2005, respectively. Similar point correlations of DJFM seasonal (c) OLR and (d) precipitation with seasonal SST anomalies are also shown. Correlation at 5% significance level is shown as black contour line. Note that the contour scale in (a) and (b) is different from that in (c) and (d).

3.2. MSSA of OLR and precipitation anomalies

The space–time structures of the dominant modes of variability of OLR were obtained by applying MSSA to daily OLR anomalies for all the days of the period 1979–2007 with a lag window of 121 days at one-day interval. The region over which the MSSA is applied to OLR anomalies covers 110 °W–0°, 50 °S–20°N. A similar MSSA was carried out separately with the daily precipitation anomalies of the period 1979–2005. Although the rain gauge data are available over a large region of the South American continent, the continuous data (without data missing even for a single day) needed at one-day interval for the MSSA of

precipitation anomalies are available roughly in the region (65 °W–35 °W, 40 °S–0°). The first few MSSA eigenmodes, arranged in descending order of the variance explained, that are above the noise level are found to consist of both oscillatory and non-oscillatory modes. The first eigenmodes of OLR and precipitation are non-oscillatory and vary on interannual time scale. These leading eigenmodes will be shown to be related to ENSO. Among the other eigenmodes, there is a mode varying on decadal time scale and related to the Atlantic SST and an oscillatory mode varying on intraseasonal time scale. Since the focus of this study is on ENSO, the subsequent discussion will be limited to the first eigenmode. The first eigenmode of OLR anomalies explains 0.9% of the total variance while that of the precipitation anomalies explains 0.8%. These values are small because the modes are extracted from daily data which consist of many scales of variability, and it is important to note that they are the leading modes. These leading modes display interannual variability on daily time scale. The MSSA was repeated with 5-day, 15-day and 31-day running means of daily OLR anomalies, obtaining the same leading mode but now with 2.0%, 4.4% and 7.4% of the total variance explained, respectively.

From the MSSA of raw daily anomalies of OLR and precipitation, the first reconstructed components (RC1s), which are simply the part of the original time series representing the first eigenmode, were constructed. RC1 is computed by using the ST-EOF (lagged maps) and the ST-PC of the first eigenmode obtained from the MSSA application (see Ghil *et al.*, 2002 for details on computing the RC). It is important to note that RC1 has the same spatial domain and time length as the original data. To examine the variance of RC1 on different time scales, CESA index of RC1 was computed by area averaging RC1 over the CESA region. The daily, monthly and DJFM seasonal averages of the CESA index of OLR RC1 account for 1.3%, 5.6% and 23.6%, respectively, of the variance of the corresponding averages of the total OLR anomaly. Thus, the first daily MSSA eigenmode explains a considerable part of the interannual variability.

The RC1s of OLR and precipitation anomalies were subjected to separate spatial EOF analysis to describe their spatial pattern and time variability. Since the first EOF (EOF1) in each case explains 99% of the total variance of the corresponding RC1, EOF1 and the first principal component (PC1) provide all the information about the spatial pattern and time variability of RC1 in a compact manner. The EOF1 of OLR RC1 shown in Figure 2(a) has an east–west gradient structure to the north of 20 °S with one sign over the eastern Pacific Ocean and opposite sign over the land and the equatorial Atlantic Ocean. There is also a north–south gradient with the change of sign occurring at about 20 °S. The daily amplitude and sign of this spatial pattern vary according to PC1 shown in Figure 2(c). The most noticeable feature of this daily PC1 is that its variability is interannual without the presence of intraseasonal or higher frequency fluctuations. In other words, during a particular season (say DJFM), this

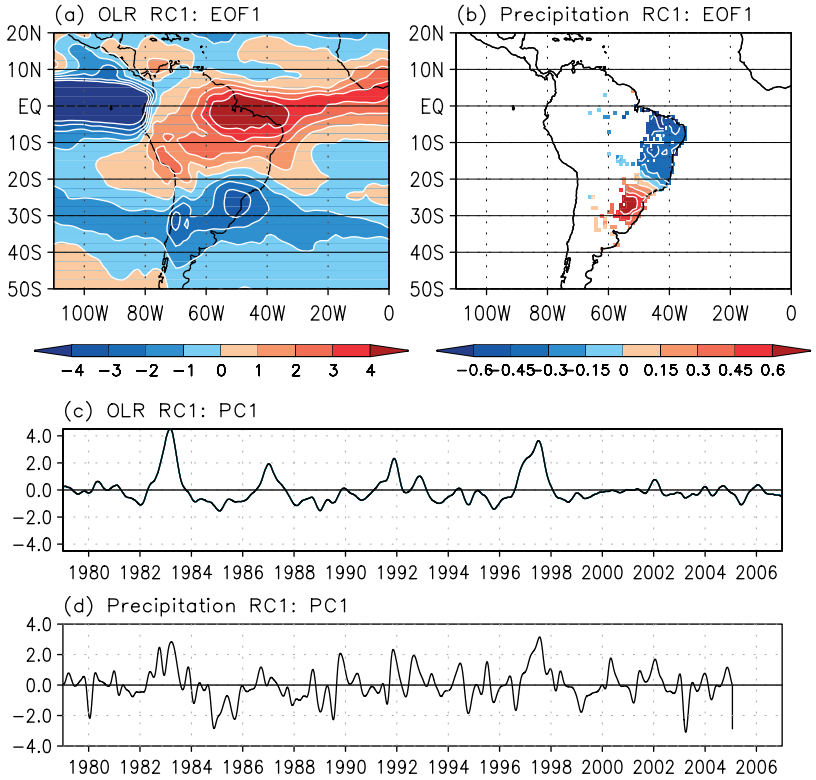

Figure 2. Spatial EOF1 of daily RC1 of (a) OLR and (b) precipitation for 1979–2007 and 1979–2005, respectively. The corresponding PC1s for (c) OLR and (d) precipitation are also shown.

mode persists with one sign. The variation of PC1 in Figure 2(c) resembles the known variation of ENSO with major El Niño events of 1982–1983, 1987–1988 and 1997–1998 being evident. The corresponding PC1s of RC1 obtained from MSSA applied to 5-day, 15-day and 31-day running mean OLR anomalies have also been plotted in Figure 2(c). However, their differences with the daily PC1 are so small that they cannot be discerned with the given graphical resolution.

The precipitation RC1 also shows the north–south gradient structure in its EOF1 (Figure 2(b)), consistent with the spatial pattern of the OLR RC1 (Figure 2(a)). The time variability of the precipitation RC1, as seen in its PC1 in Figure 2(d), also shows ENSO variability on interannual time scale. The PC1 time series of OLR and precipitation in Figure 2(c) and (d) are strongly correlated at a value of 0.75. The remarkable feature of the precipitation pattern (Figure 2(b)) is that ENSO pattern of OLR (Figure 2(a)) has been captured even without data over the Amazon River basin and over the eastern Pacific Ocean.

3.3. Relationship of the leading MSSA mode with ENSO

The CESA index (i.e. area average over CESA region) of RC1 for both OLR and precipitation is computed to find its relation with the SST anomalies. The time series of CESA index should not be confused with the PC shown in Figure 2(c). The point correlation of daily CESA index of OLR RC1 with contemporaneous daily SST anomalies during DJFM of 1982–2007 is shown in Figure 3(a). The correlation has a clear ENSO signature with the familiar horseshoe pattern. Statistically significant values cover a large region in the equatorial Pacific with most of it being in the range 0.6–0.8. These correlation values are much higher and more coherent than those of the total anomaly shown in Figure 1(a). A similar pattern with opposite sign and slightly lower values is obtained for the correlation between the daily CESA index of precipitation RC1 and SST anomalies during 1982–2005 (Figure 3(b)). These correlations suggest that El Niño (La Niña) events are associated with deficient (excess) rainfall or convective activity over CESA (north of 20 °S) and excess (deficient) rainfall to the south of 20 °S [see the dominant patterns in Figure 2(a) and (b)]. Comparing Figure 1(a) and (b) with Figure 3(a) and (b), it is obvious that total OLR and precipitation anomalies indeed consist of dominant components that are strongly related to the tropical Pacific SST and ENSO.

This seasonally persistent mode shows even stronger relation with the SST when seasonal means are considered. The point correlation of DJFM seasonal mean CESA index of OLR RC1 with the seasonal SST anomalies shown in Figure 3(c) is similar to the daily correlation in Figure 3(a) but with stronger values. In parts of the Niño-3 region, the correlation exceeds

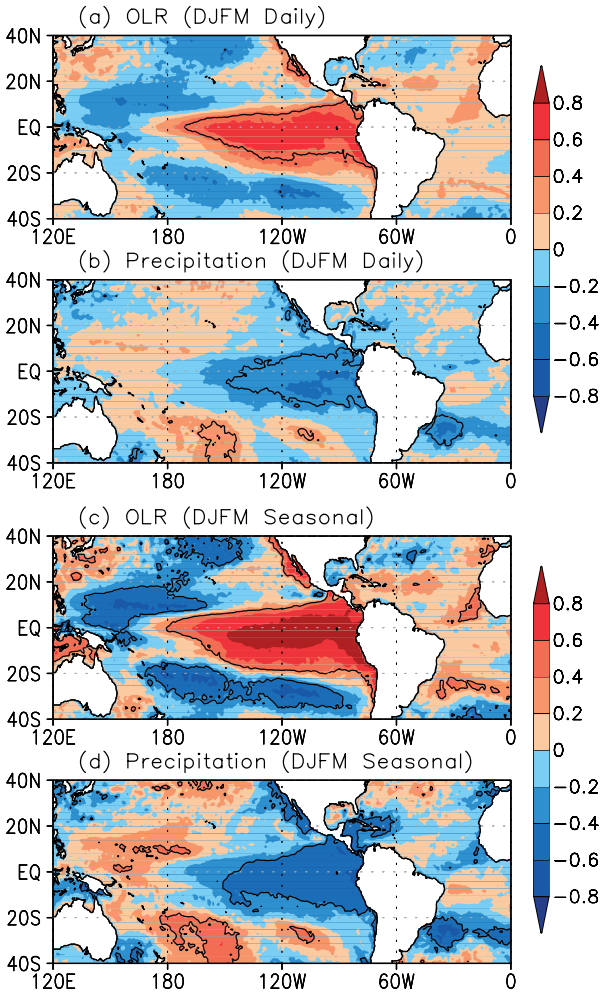

Figure 3. Point correlation of daily (a) RC1 of OLR anomalies and (b) RC1 of precipitation anomalies area averaged over the CESA region with daily SST anomalies. The periods for OLR and precipitation correlations are DJFM 1982–2007 and DJFM 1982–2005, respectively. Similar point correlations of DJFM seasonal (c) OLR RC1 and (d) precipitation RC1 with seasonal SST anomalies are also shown. Correlation at 5% significance level is shown as black contour line.

0.8. The DJFM seasonal mean CESA index of precipitation RC1 also has strong correlations with the SST in the Pacific (Figure 3(d)) with values exceeding −0.6 in the Niño-3 region. Compared to Figure 1(c) and (d), the correlations of seasonal RC1 clearly bring out the existence of ENSO-related component in the total OLR or precipitation anomalies. Interestingly, the patterns in Figure 3(b) and (d) also show negative correlations over the southwestern Atlantic, the location of the South Atlantic Convergence Zone (SACZ). The cooling in the ocean underlying the SACZ was shown to represent an ocean response to atmospheric forcing (Chavez and Nobre, 2004). The fact that both the daily and seasonal correlations are very high for the dominant modes of OLR and precipitation has implications on the role of SST in determining the seasonal mean precipitation. If the other MSSA eigenmodes, which may correspond to intraseasonal or higher frequency oscillations, do not contribute much to the seasonal mean precipitation, then the ENSO-related RC1 will

mostly determine the seasonal mean. This point is further examined by showing next the seasonal means for two specific years.

3.4. Seasonal mean anomalies

The DJFM seasonal mean of the dominant mode (RC1) is compared with that of the total anomaly for both OLR and precipitation during two specific seasons, 1997–1998 and 1990–1991. During 1997–1998, a strong El Niño year, the seasonal mean of the total OLR anomaly (Figure 4(a)) has good resemblance to the seasonal mean RC1 of OLR (Figure 4(c)) in spatial structure and magnitude. Similar resemblance between the seasonal means of total precipitation and its RC1 is seen Figure 4(b) and (d), respectively, with the north–south gradient structure of the total anomaly represented remarkably well by RC1. However, during 1990–1991, a normal (or neutral) year in the ENSO cycle, the ENSO component RC1 in the case of both OLR and precipitation (Figure 4(g) and (h)) does not adequately account for the total anomaly, although some spatial features are captured with weaker anomalies. For 1990–1991, the seasonal mean precipitation may be determined by RC1 as well as by other components such as the intraseasonal oscillations. The relative roles of the different components may play a role in the prediction and predictability of the seasonal mean precipitation.

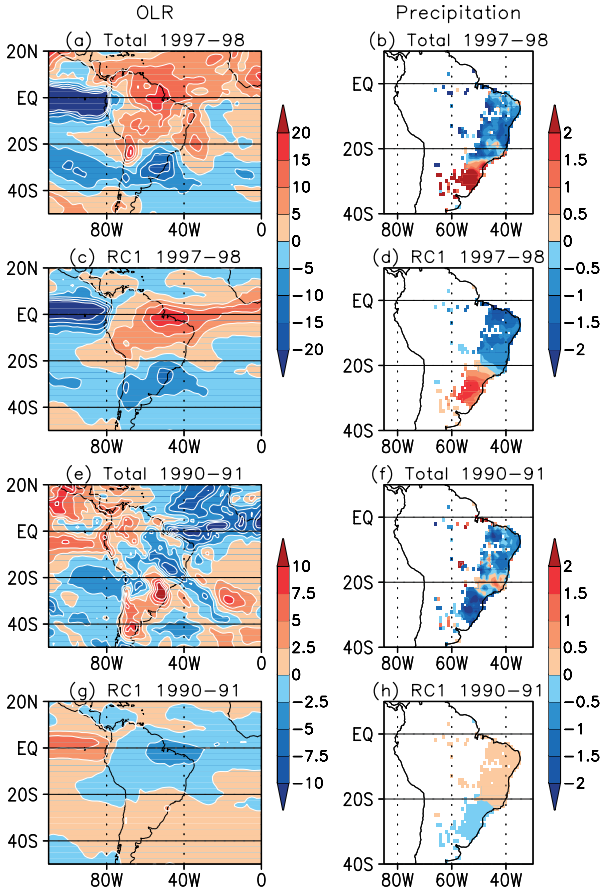

Figure 4. Seasonal means of (a) total OLR anomalies, (b) total precipitation anomalies, (c) RC1 of OLR and (d) RC1 of precipitation for DJFM 1987–1988 and a similar sequence of seasonal means for DJFM 1990–1991 in (e)–(h). Units are W m^{-2} for OLR and mm day^{-1} for precipitation.

4. Conclusions

This study has established that the leading mode of daily variability of precipitation and convection over South America consists of a regionally coherent spatial pattern that is strongly related to ENSO. This pattern explains about 0.9% of the daily variance but about 27% of the seasonal variance. The spatial pattern consists of anomalies of one sign over the eastern Pacific and region south of 20 °S and anomalies of opposite sign over the South American continent north of 20 °S (including the CESA region) and over the tropical Atlantic Ocean. This coherent pattern persists through the season with one sign and varies on interannual time scale of ENSO, describing the interannual variability of the South American atmosphere. During an El Niño (a La Niña) year, this atmospheric ENSO mode produces deficient (excess) rainfall over CESA and excess (deficient) rainfall over the region south of 20 °S. During a normal (or neutral) year of the ENSO cycle, the seasonal mean precipitation may be determined by the atmospheric ENSO mode as well as by other modes such as the intraseasonal oscillations. Shukla (1998) has, for example, suggested that the potential for long-term prediction of tropical climate exists because a part of long-term variability of the tropical climate is determined by slowly varying components such as SST. The existence of the slowly varying dominant atmospheric mode that is related to the tropical Pacific SST found in this study, therefore, provides hope for skillful seasonal prediction of rainfall in South America. However, the predictability of seasonal mean rainfall may depend on the relative roles of this dominant ENSO mode and the other (including subseasonal) modes during normal rainfall years.

Acknowledgements

This research was supported by grants from National Science Foundation (0334910), NOAA (NA04OAR4310034 and NA07OAR4310221), and National Aeronautics and Space Administration (NNG04GG46G). The authors thank Brant Liebmann for helpful comments on the manuscript and for providing the rainfall data.

References

Carvalho LMV, Jones C, Liebmann B. 2002. Extreme precipitation events in southeastern South America and large-scale convective patterns in the South Atlantic Convergence Zone. *Journal of Climate* **15**: 2377–2394.

Chavez RR, Nobre P. 2004. Interactions between sea surface temperature over the South Atlantic Ocean and the South

Atlantic Convergence Zone. *Geophysical Research Letters* **31**: L03204.DOI:10.1029/2003GL018647.

Ghil M, Allen MR, Dettinger MD, Ide K, Kondrashov D, Mann ME, Robertson AW, Saunders A, Tian Y, Varadi F, Yiou P. 2002. Advanced spectral methods for climatic time series. *Reviews of Geophysics* **40**: 1003. DOI: 10.1029/2000RG000092.

Grimm AM. 2003. The El Niño impact on the summer monsoon in Brazil. Regional processes versus remote influences. *Journal of Climate* **16**: 263–280.

Grimm AM. 2004. How do La Niña events disturb the summer monsoon system in Brazil? *Climate Dynamics* **22**: 123–138.

Krishnamurthy V, Shukla J. 2007. Intraseasonal and seasonally persisting patterns of Indian monsoon rainfall. *Journal of Climate* **20**: 3–20.

Liebmann B, Allured D. 2005. Daily precipitation grids for South America. *Bulletin of the American Meteorological Society* **86**: 1567–1570.

Liebmann B, Jones C, Carvalho LMV. 2001. Interannual variability of daily extreme precipitation events in the State of Sao Paolo, Brazil. *Journal of Climate* **14**: 208–217.

Liebmann B, Marengo J. 2001. Interannual variability of the rainy season and rainfall in the Brazilian Amazon Basin. *Journal of Climate* **14**: 4308–4318.

Liebmann B, Smith CA. 1996. Description of a complete (interpolated) outgoing longwave radiation dataset. *Bulletin of the American Meteorological Society* **77**: 1275–1277.

Reynolds RW, Smith TM, Liu C, Chelton DB, Casey KS, Schlax MG. 2007. Daily high-resolution-blended analyses for sea surface temperature. *Journal of Climate* **20**: 5473–5496.

Shukla J. 1998. Predictability in the midst of chaos: a scientific basis for climate forecasting. *Science* **282**: 728–731.

Vera C, Higgins W, Amador J, Ambrizzi T, Garreaud R, Gochis D, Gutzler D, Lettenmaier D, Marengo J, Mechoso CR, Nogues-Paegle J, Silva Dias PL, Zhang C. 2006. Toward a unified view of the American Monsoon System. *Journal of Climate* **19**: 4977–5000.

Zhou J, Lau K-M. 1998. Does a Monsoon Climate Exist over South America? *Journal of Climate* **11**: 1020–1040.

